Proceedings World Geothermal Congress 2020+1
Reykjavik, Iceland, April - October 2021

Abrasion by Particles in Suspension in Ultra High Enthalpy Geothermal Production (Super-Hot Geothermal Wells)

Heber Diez[1], Cristobal Camacho, Víctor Soria[2], Héctor Martínez[2], Felipe Solano[1] and Gabriel Luévano[1].

[1]Gerencia de Proyectos Geotermoeléctricos, CFE: Alejandro Volta 655 Morelia- Michoacán- México

[2]Instituto Tecnológico de Morelia: Avenida Tecnológico 1500, 58120 Morelia- Michoacán México.

heber.diez@cfe.gob.mx, heber.diez@outlook.com

Keywords: Abrasion, erosion, particles, silica, quartz, deposition, incrustation, corrosion, casing, materials, superheated, enthalpy, modeling, numerical simulation, CFD.

ABSTRACT

The hydrothermal geothermal wells of 'ultra-high enthalpy' (supercritical or superheated) are excellent producers. However, despite being a desired resource for their energetic conditions for electricity generation purposes, they bring multiple operational problems, such as scaling, corrosion and abrasion-erosion. This can dramatically reduce the useful life of the production well, impacting the reliability and production costs of geothermal power plants. In this research, it was demonstrated that in geothermal wells that operates in superheated thermodynamic conditions, produces highly abrasive-erosive steam, among other undesirable characteristics, attributable to suspended solids that travel in the production fluid. In spite of the different chemical reactions and operating conditions that can contribute to the degradation of the casing and the equipment in contact with the fluid, it was found that the abrasive-erosive phenomenon has the greatest impact on casing wear and it is considered that it can favor other chemical phenomena in its degradation.

In order to demonstrate the aforementioned phenomenon, the production conditions of a well with superheated characteristics were studied, physical evidence was collected in several mechanical elements (deposits) and analyzed, and at the same time an extended review of the state-of the art in experimental research on possible physical-chemical phenomena that could occur in systems under similar conditions has been carried out in order to discriminate and simplify the case of study. Subsequently, a mathematical model was developed that was solved numerically using commercial Computational Fluid Dynamics (CFD) software, and the results were validated against experimental data obtained from a mechanical element (capillary tube) that suffered serious mechanical damage after 251 hours of operation in the well under the mentioned conditions. The simulation succeeded in reproducing the abrasion-erosion phenomena that occurred in the capillary tube in a satisfactory way, and for the casing the mathematical model predicted critical mechanical damage appearing after two years of operation of the well under the reported conditions.

Therefore, it is concluded that the abrasion-erosion phenomena have a significant effect on geothermal wells operating under superheated thermodynamic conditions and a dramatic impact on their useful life, as has been observed in some geothermal wells. Therefore, it is suggested to carry on with the research on the development of new materials capable of withstanding such aggressive operating conditions.

1. INTRODUCTION

Due to the approach that has been taken at a global level regarding the promotion of the usage of clean or renewable energy, the exploitation of geothermal energy has presented a boom stage due to the benefits it presents. This has come to take center stage in the energy field of Mexico and even the world. However, although Mexico has enormous geothermal potential, current energy policies demand greater efficiency and profitability in these types of projects. Therefore, it is desirable to improve all processes during the extraction and use of this energy.

These conditions have led to the development of new exploration and exploitation techniques, in addition to those already known as low, medium and high geothermal enthalpy, opening the way for the creation of methodologies that allow the exploitation of ultra-high enthalpy geothermal resource or super-hot (superheated and supercritical) fluids. The term "ultra-high enthalpy" (Elders et al., 2014), is intended to indicate that the geothermal resource has an enthalpy substantially superior to enthalpies that commonly correspond to saturation fluids. This geothermal resource corresponds with superheated fluid which has several degrees of superheating, or in particular case "supercritical" condition, these terms are associated with high temperatures and high heat content. The latter brings great energy benefits, but for their exploitation it requires a greater investment in infrastructure. This is due to the fact above, given that during the exploitation of "ultra-high enthalpy" or "super-hot" resources, there are major problems in the facilities, as evidenced in Mexico and Iceland (Elders, 2015a; Elders and Friðleifsson, 2015; Elders; 2015b; Elders et al., 2014; Thorbjornssona et al., 2014; Markusson and Hauksson, 2015), Einarsson et al (2015). One of the main problems to which this issue has been attributed is the corrosion derived from the presence of HCl and other components. However, the present work suggests that the main component that gives rise to the deterioration of the pipes is not chemical, but mechanical. This component is the abrasive-erosive wear attributed to suspended particles that travel within the steam, with a higher hardness that of the casing of the wells. This article deals with mechanical and material phenomena, which are associated with erosion-abrasion generated by a superheated steam that contains abrasive particles in suspension (SiO_2).

Therefore, the design specifications that have been used in these wells are no longer appropriate because they deteriorate in a shorter period than the minimum required for the return on investment. However, although it is presumed that this is the problem and there are various studies looking to solve it, there is no research that gives certainty that the aforementioned is the phenomenon that degrades

these wells, particularly in Mexico. This is why the present work is proposed, with the purpose of responding if indeed the main reason for the deterioration of the mentioned pipes is due to the abrasion-erosion phenomenon, caused by particles suspended in the production steam, in addition to characterizing a more detailed behavior of this apparent phenomenon of geothermal reservoirs.

Thanks to the increase in the processing power of computers, currently it is possible to model and predict complex phenomena such as erosion, so making use of Computational Fluid Dynamics (CFD) software, we seek to propose a possible solution that allows increasing the use of this type of wells, maintaining a convenient cost-benefit ratio.

2. OBJECTIVE

Establish a study to determine basic actions in order to mitigate the degradation of casing pipe of geothermal production wells caused by suspended solids that travel in the production fluid.

3. HYPOTHESIS

Geothermal wells that operates in supercritical or superheated thermodynamic conditions produces an extremely abrasive-erosive steam, among other undesirable characteristics, this is attributed to the suspended solids that travel in the production fluid. Despite different chemical reactions and operating conditions that can contribute to the degradation of the casing pipe and the equipment in contact with the fluid, it is the abrasive-erosive phenomenon that has the greatest impact on the wear of the pipes.

4. THERMODYNAMICALLY SUPERHEATED PRODUCTION WELLS

Superheated steam wells produces a 100% steam. However, this steam has a temperature higher than saturation temperature that corresponds to the operating pressure of the system (Diez et al., 2018; Diez et al., 2015).

5. CORROSION

The corrosion process consists of the deterioration of a metallic material due to a reaction with chemicals present in the environment. Multiple processes were studied in the present work to rule out their influence on the deterioration of the well pipes under study. The studied processes are: chemical corrosion, electrochemical corrosion, pitting corrosion, stress corrosion, intergranular corrosion, and metal dusting. (Diez, 2018; Karlsdottir et al., 2014, Banaś et al., 2007, Paz and Grabke, 1993; Devan et al., 1997, Alan, 1995; Thorbjornsson et al., 1995, Roauaix, 2015).

6. EROSION

The erosion of metallic materials is attributed to two types of damage. One is the removal of material due to repeated plastic deformation and the other is due to shear stress. These processes occur at the same time, and the ratios at which these processes contribute to total damage depends on both the angle and speed of impact, as well as the physical and mechanical properties of the particles and the impacted material. Therefore, erosion resistance is not an intrinsic property of the material. The erosion resistance of a material depends on the tribological system in which it operates and is different for fragile and ductile materials (Diez, 2018; Kirchgaßner, 2008; Treviño, 2009; Akhihiro et al., 1999; McCabe et al., 1985; Duarte et al., 2015).

Hardness is the most used parameter in mathematical models, but insufficient as a single property of the material, and does not apply to all erosion systems (Meng and Ludema, 1995).

7. CHARACTERISTICS OF THE WELL UNDER STUDY

7.1 Operating Conditions of The Well

The well under study showed a superheated steam production of approximately 68 °C (Table 1).

Table 1: Operating conditions of the well (CFE).

Well operating conditions	
Orifice plate	50.8 mm (2") Ø
Estimated production	35 t/h of superheated steam
Well head pressure	40 barg (585 psig)
Well head temperature	320 °C (~)
Superheating	68 °C (~)

7.2 Chemical Analysis of the Production Fluid

The chemical analysis of the liquid and gas phases of the production fluid, corresponding to the operating conditions described in Table 1, are shown in Tables 2 and 3.

Table 2: Results of the chemical condensate analysis (CFE).

Chemical composition of the condensate													
pH	Electrical conductivity (S/cm)	Total Alkalinity (meq/l)	Cl	B	HCO_3	SiO_2	SO_4	Na	K	Ca	Mg	As	Fe
			meq/l (ppm)										
4.47	145	0.4266	31	958	1.67	21.95	45	0.58	0.36	0.55	0.04	9.11	8.21

Table 3: Results of the chemical analysis for non-condensable gases [CFE].

Weight percentage of gases								
Total Gas (%WT)	AR	CH_4	CO_2	H_2	H_2S	He	N_2	NH_3
3.86	0.77	0.013	84.81	0.4	9.62	0	4.891	0.004

7.3 Mechanical Characteristics of the Well

Figure 1 shows the mechanical configuration of the construction of the well under study, as well as an extract of the mechanical tests carried out on the installed pipe after its manufacture (Figure 2). The pipes that are in direct contact with the fluids of the well with typical termination are the 244 mm (9 5/8") diameter production casing and the 177 mm (7") diameter blank and slotted liner. The mechanical properties of the pipes used were obtained from the data provided by the manufacturer (Tenaris TAMSA). The hardness of these pipes is generally around 19 points on the Rockwell C (HRC) scale.

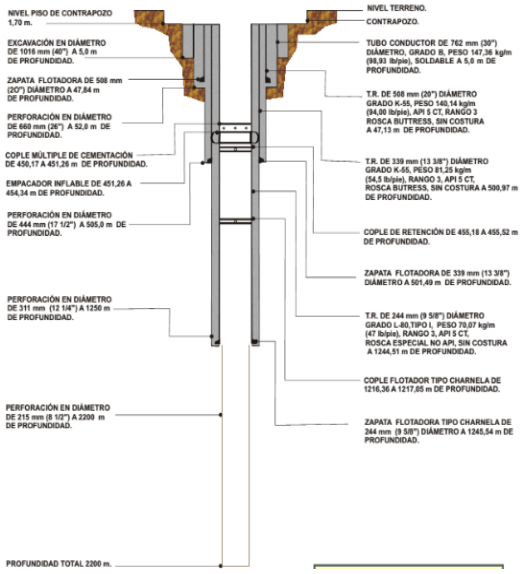

Figure 1: Mechanical state (CFE).

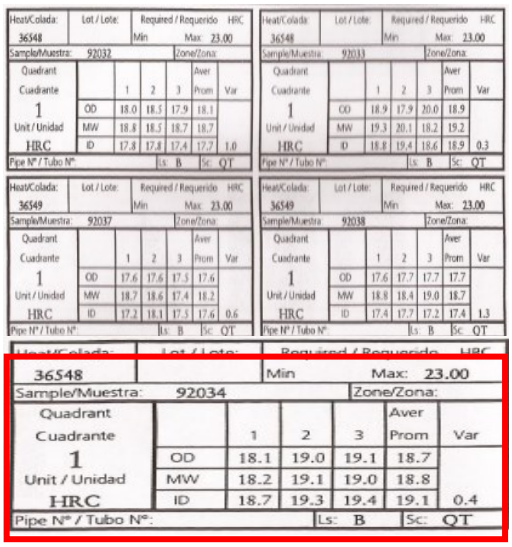

Figure 2: Extract essay of materials (CFE).

8. EVIDENCE OF THE DEGRADATION OF THE CASING PIPE

During a time of discharge and operation of the well under the conditions described above, a deposition of a ferrous and probably amorphous material in the mechanical elements exposed to its fluid was observed on different instances. Derived from the above, multiple samples were collected and in turn characterized. Part of the samples studied were collected from the restriction orifice plate and filter for solids that formed part of the surface installations of this well (Figure 3).

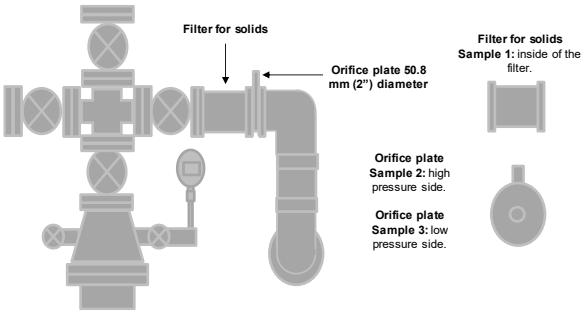

Figure 3: Mechanical elements that presented deposited material.

Figure 4: Filter for solids (top), high pressure side hole plate (center) and silver low-pressure side hole (bottom) (CFE).

The appearance of the collected samples and the mechanical elements in which the deposition or "scale" was found, are shown in Figure 4. In descending order: filter for solids (Sample 1), orifice plate side of high pressure (Sample 2) and low-pressure side orifice plate (Sample 3). Samples 1 and 2 have similarities in appearance; the sample is made up of compact fine grain plates. The pressure and temperature conditions to which they were subjected are those indicated in Table 1. Sample 3 was collected on the low-pressure side. Its appearance is somewhat different and the thermodynamic conditions at that point were 10.34 barg, 255 °C, and 70°C of superheat.

9. CHARACTERIZATION OF DEPOSITED MATERIAL

The characterization of the solid material deposited was carried out by personnel of the Federal Electricity Commission (CFE) and the Institute of Electrical Research (IIE), now the Institute of Electricity and Clean Energy (INEEL), of the Testing, Equipment and Materials Laboratory (LAPEM) of the CFE and the Technological Institute of Morelia (ITM), carrying out chemical, petrographic, X-ray Diffraction (DRX), Scanning Electron Microscopy (SEM) and Energy Disperse Spectroscopy (EDS) particle analysis deposited in the orifice plate on both the high pressure and low pressure sides (Figure 4).

9.1 Chemical Characterization of Deposited Samples

The chemical analysis carried out in the field yielded the following results (Table 4).

Table 4: Chemical analysis of deposited samples (CFE).

Orifice plate 50.8 mm (2") diameter					
High pressure side			Low pressure side		
Compound	ppm	%	Compound	ppm	%
FeO	37.86	6.57	FeO	1.223	0.21
As_2O_3	2.17	0.14	As_2O_3	17.18	1.11
H_3BO_3	0	0.00	H_3BO_3	0	0.00
$NaCl_3$	18.93	2.39	NaCl	0.679	0.09
SiO_2	694	34.49	SiO_2	518	25.64
KCl	19.29	1.83	KCl	2.139	0.20
LiOH	0.033	0.006	LiOH	0.066	0.011
$MgCO_3$	0.141	0.02	$MgCO_3$	0.127	0.02
$CaCO_3$	0.92	0.11	$CaCO_3$	1.062	0.13
		45.57			***27.41***

From the table above, we can observe the ratio of measured compounds. However, by paying attention to those of particular interest to us, it is noted that silicon dioxide (SiO_2) appears in a considerable amount on each side of the plate. When observing the "iron oxide (FeO)", it can be seen that on the high-pressure side the quantity is much greater than on the low-pressure side.

9.2 Petrographic Characterization of the Samples

The petrographic analysis was carried out on different samples by staff of the geology area of the CFE, determining the following that the analyzed samples are constituted by an amorphous and euhedral silica, mainly by tridymite and to a lesser extent cristobalite. (Figure 5). (CFE).

Figure 5: Microscope image of the sample of deposited material (CFE, Diez et al., 2018).

9.3 X-ray diffraction (DRX)

The IIE, supported with the characterization of the samples of the orifice plate, high- and low-pressure side applying X-ray diffraction. In the result of the high-pressure side (Figure 6), several types of Fe oxides can be identified, mainly magnetite, and most likely wustite and pyrrhotite. As for the low-pressure side (Figure 7), a mass corresponding to an "amorphous material" can be identified, probably silica, in addition to finding halite and possibly pyrite.

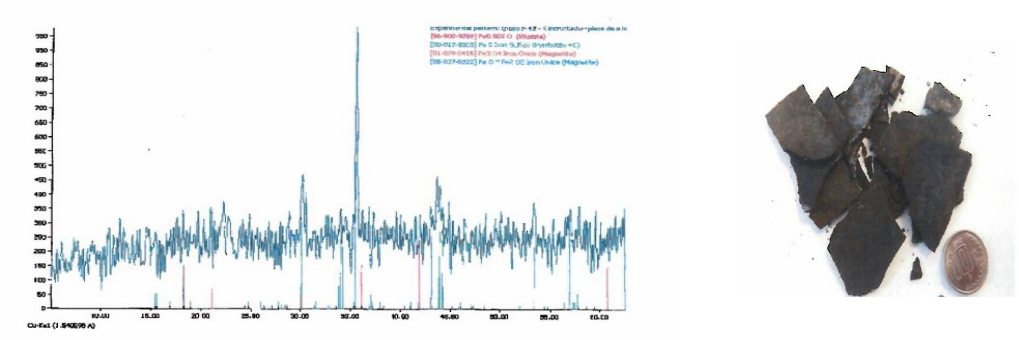

Figure 6: DRX Sample collected from the high-pressure orifice plate (CFE).

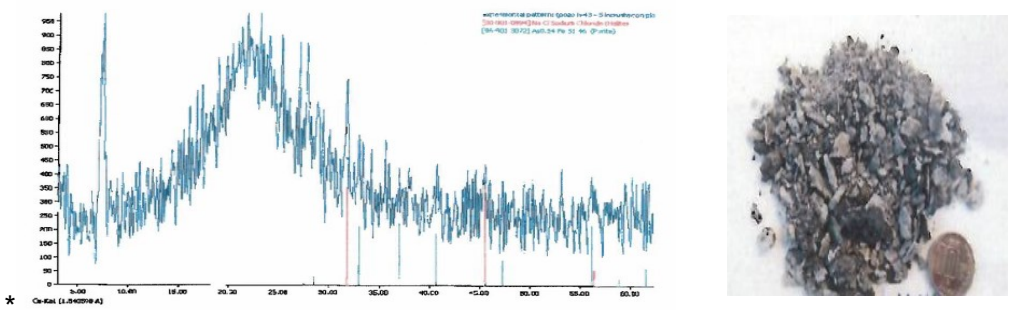

Figure 7: DRX Sample collected from the low-pressure orifice plate (CFE).

9.4 Scanning Electron Microscopy (SEM) and X-Ray Energy Dispersion Spectrometry (EDS)

Through the LAPEM laboratory, a series of analyses were performed on the corresponding samples (Figure 8). To deepen the study, some analyses were carried out with the Technological Institute of Morelia (ITM), on the same samples (Figure 9).

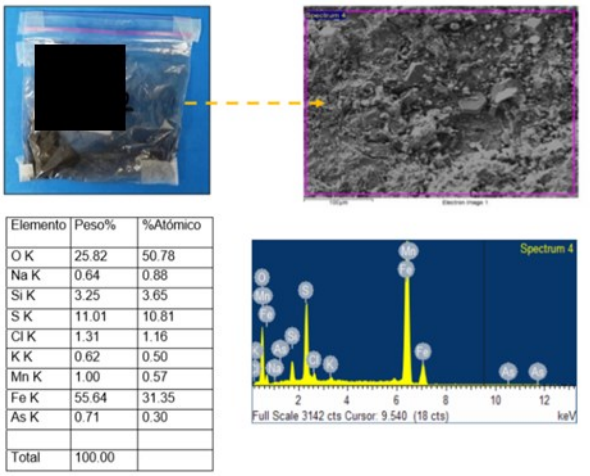

Elemento	Peso%	%Atómico
O K	25.82	50.78
Na K	0.64	0.88
Si K	3.25	3.65
S K	11.01	10.81
Cl K	1.31	1.16
K K	0.62	0.50
Mn K	1.00	0.57
Fe K	55.64	31.35
As K	0.71	0.30
Total	100.00	

Figure 8. Filter for solid analysis SEM-EDS, LAPEM (CFE).

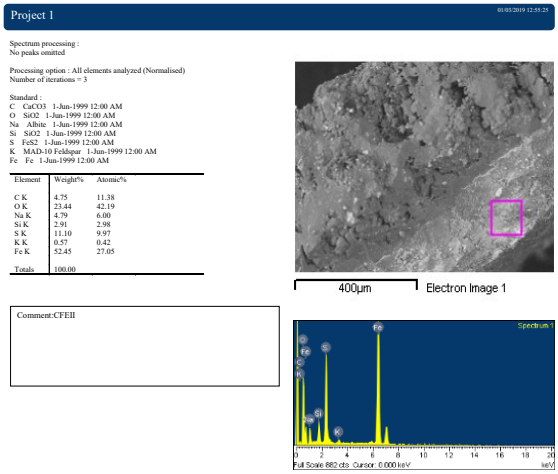

Figure 9. Filter for solid analysis SEM-EDS, ITM.

Additionally, a well was designed and built on the same platform as the one in this study, with some differences, including the characteristics of the casing pipe different from the conventionally used L80. This pipe was a TN80 3% Cr resistant to CO_2-rich environments. That is, resistant to "corrosive" conditions. However, during the operation of this well, there was a decline in its production attributed to a scaling process due to the presence of permeable zones with different thermodynamics (Diez, 2019). Subsequently, a scale sample between 1,135 m and 1,140 m was recovered and the presence of metal powders, attributable to the TR of 177 mm, was observed. Therefore, it was decided to analyze through SEM and EDS in the ITM, finding the following results (Figures 10 and 11):

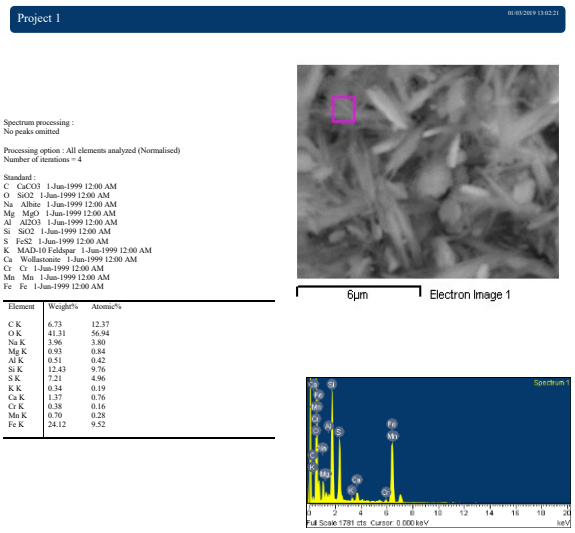

Figure 10. Downhole sample 1 SEM-EDS, ITM.

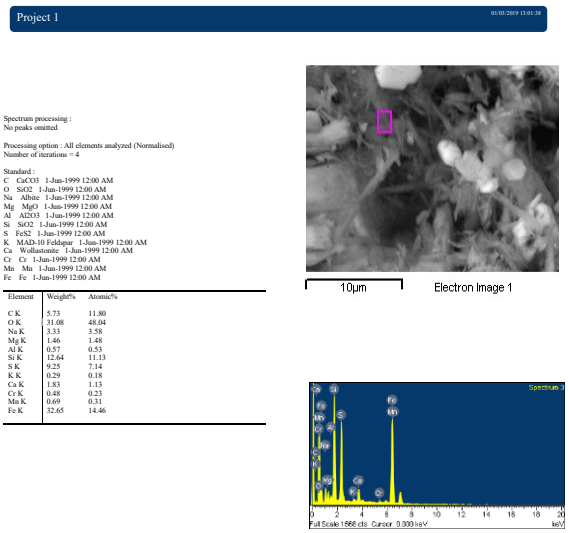

Figure 11: Downhole sample 2 SEM-EDS, ITM.

Of the analyzed samples corresponding to L80 casing, the results of the IIE and LAPEM show the presence of oxides and sulfides, from which the presence of corrosive processes and even hydrogen embrittlement can be presumed. However, the samples analyzed by the ITM, although they also show evidence of corrosion, it was possible to detect detachment metal and elements attributable to the chemical composition of the casing, its detection is linked to an erosion phenomenon, rather than corrosive phenomena. It is emphasized that a search criterion for particles was applied. Regarding the analyzed sample of the TN80 3% Cr TR, applying the same particle search criteria, multiple elements of the chemical composition of the casing pipe were found, indicating again potential erosive phenomena.

9.5 Characterization of Erosive Material

Due the evidence of material deposited in the mechanical elements showed in figure 4, there is possible that exist different crystallographic phases of SiO_2, like cristobalite, tridymite and quartz, the corresponding hardness ranges from 6.5 to 7 Mohs, which is equivalent approximately to 50 or 60 HRC (Figure 12). The estimated particle size of the sample is 0.05 mm. The amount of SiO_2 that has been measured in the steam is at least 22 ppm, regarding to 35 t/h of superheated steam. Based on this measurement, the erosive flow rate in the mixture with the steam is 0.77 kg/h = 18.48 kg/day. Considering the description in the figure 5, it is possible that the more representative phase it is tridymite as a possible stable phase of SiO_2, corresponding to minuscule euhedral crystals.

10. COMPARISON OF THE HARDNESS OF THE PIPES AND THE EROSIVE

The hardness of the casing pipe grades L-80 and TN-80 3% Cr (resistant to corrosive environments), are around 19 to 23 points of hardness Rockwell C (HRC), according to manufacturer data sheets (CFE). SiO_2 is a material that in the Mohs scale of mineral hardness varies between 6.5 and 7, which is equivalent to a hardness between 50 and 60 HRC, according to its crystallographic phase. It is a reliable indication that SiO_2 crystals are potentially causing erosion in well pipes (Figure 12):

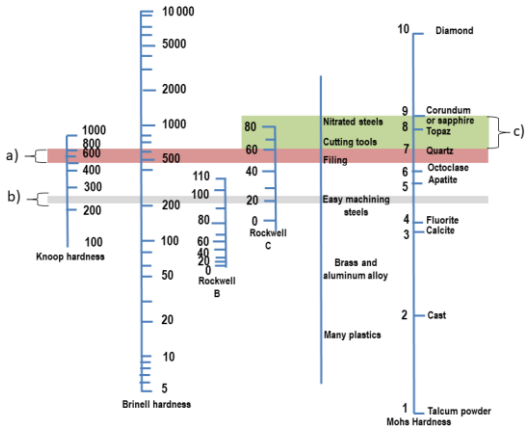

Figure 12. Hardness comparison, with a) SiO_2 hardness range, b) hardness interval of L-80 and TN-80 steels, and c) higher hardness than SiO_2 achieved with treatments (Metals Park, 1987).

11. DESCRIPTION OF THE GEOTHERMAL SYSTEM UNDER ANALYSIS

There is a geothermal system whose conditions and configuration are close to those shown in Figure 13. The operating conditions, mechanical characteristics, properties of the fluids, as well as the suspended particles, were obtained through the analyses described. In addition, it is important have present that this system corresponds to a geothermal well which produced superheated steam, no present liquid phase, so the SiO_2 that was measured on the surface traveled in the steam.

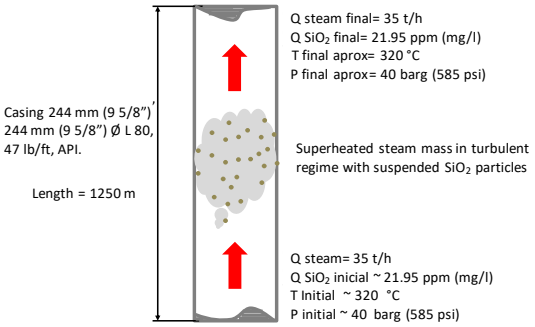

Figure 13: Schematic representation of modeling (Diez, 2018).

Due to the physical and chemical characteristics of geothermal reservoir fluids, it is believed that a large number of particles travel through superheated steam at high speeds. Some of these particles have a higher hardness greater than that of the API L-80 casing, causing erosion to its internal walls. It is noted that the hardness of the TN3% Cr TR is similar to the API L-80.

12. CONSTRUCTION OF THE NUMERICAL MODEL

12.1 Considerations, Assumptions and Simplifications.

- The problem is considered in a stable state as a first approach to solving this complex Multiphysics problem.

- The fluid flow is considered to be fully developed due to the sufficient length of the pipeline in addition to the analysis point being sufficiently far from the inlet region.
- Because the Reynolds number in question exceeds the critical Reynolds value for pipes by a very large margin, the flow was considered turbulent.
- The fluid will be considered compressible because operation records show speeds greater than Mach 0.3.
- Chemical phenomena (corrosion) will be neglected as possible cause of damage to the pipe, because it was analyzed and its effects are unlikely to occur at the beginning.

12.2 Ruling Equations

- Continuity equation
- Navier-Stokes equations
- Energy conservation equation.
- k-ε realizable model.
- Tulsa model depending on the angle.

12.3 Border Conditions

- Based on the configuration proposed in Section 11, for the capillary pipe, five boundary conditions were proposed (Figure 14).
- Non-slip Wall type condition for the outer wall of the capillary tube, with a reflective type condition.
- Non-slip Wall type condition for the inner wall of the steel casing tube, with a reflective type condition.
- Area of fluid circulation in the volume between the two pipes.
- A mass input flow of 9.72 kg/s composed of water vapor and gases, in which suspended solids travel.
- An operating pressure output of the manometric system similar to that of the inlet.

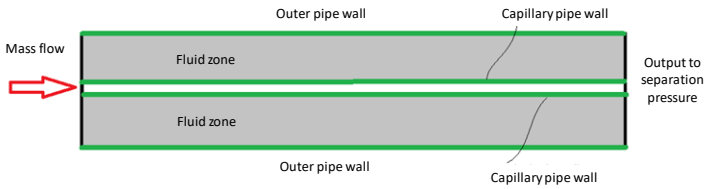

Figure 14: Border conditions (Diez, 2018).

13. COMPUTATIONAL MODEL

In order to corroborate the hypothesis, the geometry of Figure 14 was modeled, where the described boundary conditions were raised, loading to the software with the considerations to assess the erosion phenomenon. Defining an injection of silica particles of discrete phase, particle size and geometry (not spherical or with sharp edges) and mass flow was established, among others, see Figures 15, 16 and 17.

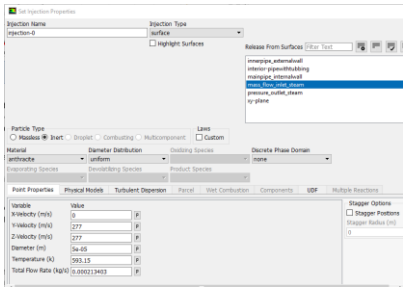

Figure 15: Configuration of discrete phase model parameters (Diez, 2018).

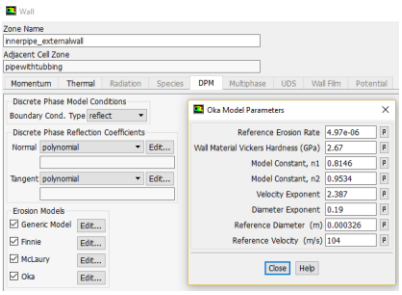

Figure 16: Configuration of the Oka model in Ansys for the capillary tubing (Diez, 2018).

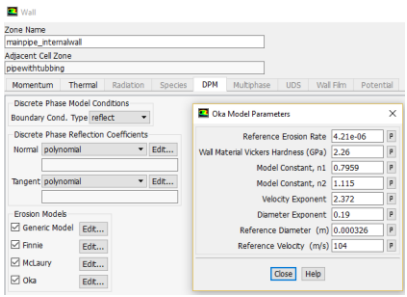

Figure 17: Configuration of the Oka model in Ansys for casing (Diez, 2018).

The "OKA Erosion Model" was used to evaluate erosion in the capillary tubing, considering its geometry and physical characteristics. It was subsequently calibrated and applied to evaluate the performance of the L80 casing pipe. It is important to note that the chemical parameters were discarded, since it was considered that the reactions that could be carried out do not take place in the physical chemical conditions of the system, simplifying the analysis.

14. VALIDATION OF THE COMPUTATIONAL MODEL BY OPERATIONAL EXPERIENCE

Originally the design of an experimental prototype was proposed to evaluate the erosion in a specific material in order to obtain results of its behavior when subjected to the fluid of one of the geothermal wells under study (in this case the one that was built in the same platform). The results would be used to observe the percentage of error in the simulation, and thereby calibrate the numerical

model. Due to a delay in the commissioning of the selected well and subsequent operational problems in it, it was not possible to perform the indicated tests. Derived from the above, it was necessary to make a documentary review of the well that motivated the present study, and useful information was detected for this section of the investigation. Finding that during a dosing test of NaOH (HCl-neutralizing fluid) inside the well, a failure in the pumping system was observed, manifesting variations in the fluid injection pressure. This can be seen in the first orange box of Figure 18 that highlights the unstable behavior of the system, which suggested the loss of material due to the increase in the equivalent cross-section of flow, resulting in the drop in pumping pressure (red line). In the second orange box of the same figure, the pressure drop related to having lost 400 m of capillary tube is shown. When recovering part of the capillary tube, material loss of up to 100% was detected as shown in Figure 19.

It is important to highlight that the material of the 9.525 mm (3/8") Ø capillary tube used was a high-alloy multi-purpose austenitic stainless steel highly resistant to the following conditions: corrosive environments, stress corrosion cracking, intergranular corrosion in various environments, pitting and cleft. However, after commissioning the neutralization system, it presented the failures described in the pumping system. Therefore, and according to an internal analysis of the CFE, it was indicated that the capillary tube failure was caused by a corrosive phenomenon: stress corrosion cracking, but when conducting a thorough review, the possibility that an abrasive phenomenon promoted the loss of material and allowed the corrosive phenomenon was detected.

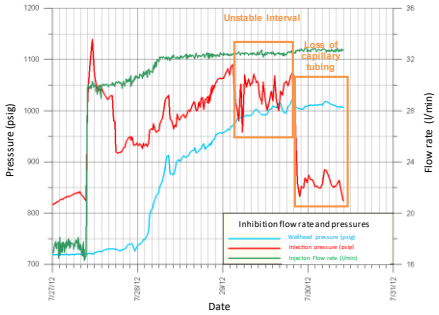

Figure 18: Operation graph (time vs pressure vs flow rate) (CFE).

Figure 19: Extract of capillary tubing recovered after failure (CFE).

Therefore, it was assumed that the failure must have been caused by an erosive process on the dosing pipe, since it presented a gradual thinning in its thickness and total losses of material with erosion topology. In order to calculate an erosion rate to compare and calibrate the mathematical model, a stress analysis was performed to calculate the minimum thickness that the pipe had to endure before failing. The minimum thickness that the capillary tubbing could support before failing and losing 400 m in length was determined, plus the bottom hole dosing fittings, should be t = 0.01753 mm. Taking into account that the behavior of the injection pressure was stable from day 18 until July 29, 2012 (Figure 18), it is considered that at that time there was a pressure drop due to a depressurization caused by the increase in the area of NaOH flow. The above was attributed to the loss of material in the body of the capillary tubing (Figure 19). Therefore, it was estimated that the time in which 0.889 mm of thickness of the capillary tubing wall disappeared, manifesting the depressurization of the system, was 251 hours. With these data, we proceeded to calculate the erosion rate associated with the described event, corresponding to 31.03 mm/year. Subsequently, the time in which the minimum thickness calculated analytically would be reached was estimated (t = 0.01753 mm). Analyzing the parameters involved, it was determined that the minimum thickness for failure would be reached within 247 and 248 hours, very close to those observed, with respect to the variations recorded in the pump system (251 hours). Given the results obtained, the erosion rate of 31.03 mm/year in the capillary tube was considered valid to compare and calibrate the results that would be obtained with the numerical model.

It is important to highlight that, in the previous analysis, there are other forces, such as the thrust force generated by the flow of steam when coming into contact with the cross section of the bottom rig. However, for practical purposes, it was considered that these can be neglected.

15. ANALYSIS AND DISCUSSION OF RESULTS

Once the variables and constants were loaded, the solution of the model was initialized. The simulation was run, and after 236 iterations it converged, and the residuals of speed and turbulence were satisfactory. Post-processing of the results obtained from the first approximation of the simulation showed preliminary data of maximum fluid velocity in 339 m/s, in the Figure 20 the velocity profile of the boundary layer and velocity distribution can be seen. The simulation results were calibrated based on the results obtained from the experimental erosion rate. This involved adjusting the value for the average system speed, which corresponds roughly to the theoretical calculations of an average turbulent flow velocity of 270 m/s. The result was to obtain a maximum erosion rate of $7.76E10^{-6}$ kg/m²-s, which is equivalent to 30.58 mm/year of material loss (Figure 21). It should be noted that the results obtained in the fault

zone, where the highest erosion rate is found (Figure 21), show a great resemblance to the damage presented by the capillary tube recovered after the failure described in Figure 19.

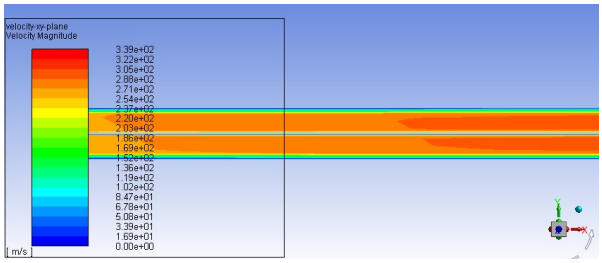

Figure 20: Estimated velocity profiles obtained from computational simulation, capillary tube (Diez, 2018).

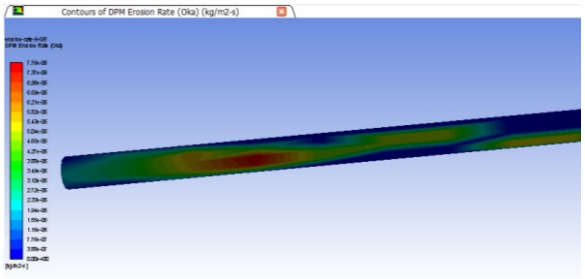

Figure 21: Estimated contours of erosion speed for capillary tube (Diez, 2018).

Once the model for the capillary tube was calibrated, the erosion rate for the casing pipe was evaluated. Post-processing yielded the velocity profile shown in Figure 22, reaching a maximum value of 339 m/s, which confirms the suspicion that the fluid will reach speeds close to those initially assumed and a maximum erosion rate of 1.59 x106 kg/m2-s, equivalent to 6.277 mm/year. If we consider the pipe wall thickness around 12 mm (supplier data), then the simulation result suggests that in approximately two years the casing pipe would begin to present critical failures in various sections, as shown in Figure 23.

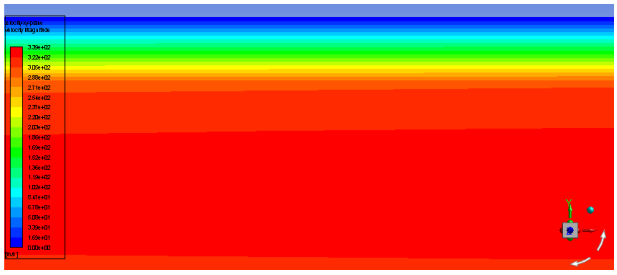

Figure 22: Estimated velocity profiles obtained from computational simulation, casing pipe (Diez, 2018).

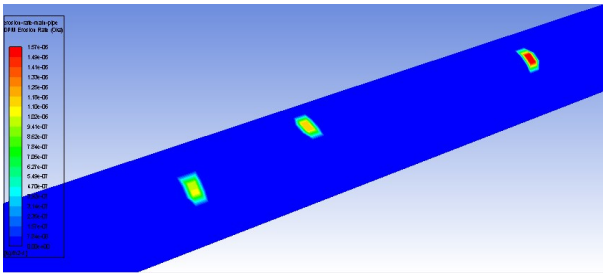

Figure 23: Estimated erosion rate for the casing tube (Diez, 2018).

Derived from the above, the following is discussed: the well produces 35 t/h of steam with at least 68 °C of superheat at a wellhead pressure and temperature of 40 barg (585 psig) and 320 °C, respectively. After reviewing the chemical composition of the condensate, we observe that it has 21.95 ppm of silicon oxide (SiO_2), among other chemical elements. SiO_2 is a mineral which in the Mohs scale of mineral hardness corresponds between 6.5 and 7 points, of a maximum of 10, the latter corresponding to diamond. Preliminarily comparing the Mohs value of SiO_2 with the Rockwell C scale, it is observed that SiO_2 is higher in hardness than the pipe. This is corroborated by the certificates of mechanical hardness tests performed on the casing, which highlights Rockwell C hardness of 19 points, on average. The above is a first indication that the problem has a high probability of being generated by suspended solids that travel in the production fluid through the well pipe, degrading it. The chemical, petrographic, DRX, SEM and EDS analyze showed the presence of SiO_2. Apparently, in this case, tridymite turned out to be potential representative mineral and, given its proportion, to which the erosion of the pipes is attributed. Although part of the results indicates the presence of oxides and compounds of possible corrosion phenomena, including hydrogen embrittlement, the truth is that there is evidence of the presence of erosive phenomena supported by the observation of detachment metal and elements of composition of the casing pipe. Erosion is explained due to the presence of SiO_2, in the absence of a lubricating medium. Regarding the oxides, it can be assumed that it is a detachment metal that reacts chemically with the well fluid. The presence of sulfides (hydrogen embrittlement indicators), can be attributed to the pipes losing the passive layer of oxides and becoming susceptible to react chemically with the H_2S gas, as with the detachment metal, the best example in this study is provided by the behavior of the capillary tube that we studied, since its super alloy characteristics withstand those corrosion conditions, but being exposed to a tribological system, where the erosive material constantly removes the passive layer of oxides, allowed corrosion and embrittlement by hydrogen as indicated in this document.

The numerical model that was developed contains all the variables, parameters and equations required to solve the erosion model. The results obtained are revealing the phenomenon that is supposed to be occurring. However, although it was not possible to carry out an experiment with specimens exposed to the well fluid, the analysis of the capillary tube failure yielded important information

to understand the erosive phenomena and allowed the model calibration. Then, was successfully reproducing the simulation for capillary failure and from which the similarity of the numerical results with the real ones can be observed. Finally, the simulation, after calibration, yielded results of the erosion rate for the casing pipeline of our interest, blunt and highly reliable.

16. CONCLUSIONS

The deposits of scaling material in certain mechanical components, was evidence of the high levels of SiO_2 present in the geothermal fluid, in addition the iron present in the scale comes largely from the degraded walls of the casing pipe. From the integral analysis of the information obtained through chemical tests, petrography, DRX, SEM and EDS, it is observed that the erosive potential is a phase of SiO_2, possible tridymite. Likewise, it can be safely assumed that the detected and analyzed powders come from the casing pipe due to an erosion process.

The hardness of SiO_2 particle (possible tridymite) is higher than that the studied pipes (casing), hardness it is a determining property during the erosion phenomenon. Any crystallographic phase of SiO2, could not make a substantial difference; the reason, it is because numerical model considered sharp edges (not really a specific shape), being the hardness the variable determinant.

The steel used in the pipe has the expected performance for the required standards as far as corrosion is concerned, under the medium in which it is located. However, the hardness of the material is insufficient to resist the effects of the impact of SiO_2 particles.

The assumption of neglecting corrosive phenomena of any kind seems to be correct, because the results obtained in terms of material degradation were as expected considering only the erosive phenomenon as the main and determining component of pipe wear. The documented failure of the capillary tube served as a point of comparison to calibrate the mathematical model, in addition to corroborating that the cause of the failure during its operation in the field was the erosive phenomenon, and subsequently the corrosive one and not as initially stated: stress corrosion cracking. The results obtained, qualitative and quantitative, for the erosion rate were quite close to the operation records. In addition, the observations derived from the behavior of the TN803% Cr grade RT designed for corrosive environments rich in CO_2, and the results of the analysis of the samples obtained between 1,135 m and 1,140 m, are another indicator of the erosive potential of the production fluid of these wells.

The use of CFD software allowed us to reproduce complex phenomena such as erosion, as long as the system is reliably modeled. In addition to that, by making the correct assumptions, it is possible to reduce the computational cost without sacrificing precision in the results.

The correctly validated model allowed us to obtain erosion values for the casing pipe, verifying that it suffered a degradation that exceeds the recommended values, which reduced its useful life prematurely over the corresponding technical and economic projection. Based on everything described in this paper, the hypothesis presented was conclusively demonstrated.

17. FUTURE WORK

Perform the design of an experiment with controlled variables to increase the accuracy of the mathematical model. Model various commercially available materials to appreciate the dependence of the erosion rate on the hardness of the pipe. Investigate the development of viable methods to increase surface hardness inside the casing pipes. Simulate the effects by varying the geometry and mechanical characteristics of the pipes, for example, the thickness. Design equipment to reduce surface erosive effects, etc.

A study is currently underway on the thermodynamic behavior of the reservoir where the wells under study are located, and its relationship with the contribution of SiO_2 in the superheated fluid. This will allow us to define the mechanical and construction characteristics of this type of well.

The above seeks to solve the problems associated with the Ultra High Enthalpy or Super-Hot wells, such as some that exist in Mexico, Iceland, and surely other parts of the world, improving their performance and finding an option that is technically and economically viable before the erosive phenomenon

18. ACKNOWLEDGMENTS

To colleagues in the field of Geothermal-electric Project Management and their RLH of the Federal Electricity Commission, to LAPEM staff, to INEEL staff and particularly to the Technological Institute of Morelia.

REFERENCES

Elders, W. (2015, April): A proposal to promote the development of higher enthalpy geothermal systems in the USA. In *Proceedings,* World Geothermal Congress.

Elders, W. A., & Friðleifsson, G. Ó (2015). Investigating a Mid-Ocean Ridge Hydrothermal System on Land: the Iceland Deep Drilling Project on the Reykjanes Peninsula in SW Iceland. In *Proceedings,* World Geothermal Congress.

Elders, W. A. (2015, January). The potential for on-and off-shore high-enthalpy geothermal systems in the USA. *In Proceedings* of the 40th Workshop on Geothermal Reservoir Engineering, Stanford University, Stanford, CA, USA 26-28.

Elders, W. A., Nielson, D., Schiffman, P., & Schreiner Jr, A. (2014). Investigating ultra-high-enthalpy geothermal systems: a collaborative initiative to promote scientific opportunities. Scientific Drilling, 18, 35.

Thorbjornssona, I. O., Karlsdottir, S. N., Einarsson, Á, & Ragnarsdottir, K. R. (2015). Materials for Geothermal Steam Utilization at Higher Temperatures and Pressure. *In Proceedings* World Geothermal Congress, Melbourne Australia.

Markusson, S. H., & Hauksson, T. (2015). Utilization of the Hottest Well in the World, IDDP-1 in Krafla. *In Proceedings* World Geothermal Congress.

Einarsson, K., Sveinsson, K. E., Ingason, K., Kristjansson, V., & Holmgeirsson, S. (2015). Discharge testing of magma well IDDP 1. *In Proceedings,* World Geothermal Congress (p. 13).

Diez, Magaly Flores, Miguel Ramírez, Rigoberto Tovar, Cesar Rosales, Felipe Solano and Fernando Sandoval. "Neutralization of Acid Fluids from Well H-43 (Superheated Steam), Los Humeros Geothermal Field, Mexico". *Proceedings* World Geothermal Congress 2015 Melbourne, Australia, 19-25 (April 2015).

Karlsdottir, S. N., Ragnarsdottir, K. R., Moller, A., Thorbjornsson, I. O., & Einarsson, A. (2014). On-site erosion–corrosion testing in superheated geothermal steam. *Geothermics*, 51, 170-181.

Banaś, J., Lelek-Borkowska, U., Mazurkiewicz, B., & Solarski, W. (2007). Effect of CO2 and H2S on the composition and stability of passive film on iron alloys in geothermal water. Electrochimica Acta, 52(18), 5704-5714.

M. Kirchgaßner, E. Badisch b, F. Franek. "Behaviour of iron-based hardfacing alloys under abrasion and impact". *El Sevier*, *Wear.* 265. 7. March (2008).

Berndt, M. L., & Philippacopoulos, A. J. Corrosion Control.

Duarte, C. A. R., de Souza, F. J., & dos Santos, V. F. (2015). Numerical investigation of mass loading effects on elbow erosion. Powder Technology, 283, 593-606.

Informe Interno Comisión Federal de Electricidad (CFE)

Hardness Testing, ASM Internationals, Metals Park, OH, (1987).

J.H. DeVan, P. F. Tortorelli, R. R. Judkins and I.G. Wright. (February 1997). Carbon Formation and Metal Dusting in Advanced Coal Gasification Processes. Oak Ridge National Laboratory, 31.

Paz, J. N., & Grabke, H. J. (1993). Metal dusting. Oxidation of metals, 39 (5-6), 437-456.

Mario E. Treviño. December (2009). Estudio del desgaste por erosion en aleaciones de baja densidad *(Tesis de Maestría*). Universidad Autónoma de Nuevo León.

Yabuki Akhihiro, Matsuwaki Kazuo, Matsumura Masanobu. "Critical Impact Velocity in the Solid Particles Impact Erosion of Metallic Materials". Wear, (1999). 468-475.

McCabe Laura, Sargent Gordon, Conrad Hans: "Effect of Microstructure on the Erosion of the Steel by Solid Particles"; *Wear* (1985) 20.

Levy Alan V. "Solid Particle Erosion and Erosion-Corrosion of Materials". ASM (1995).14.

Meng H.C., Ludema K.C. "Wear Models and Predictive Equations: Their Form and Content"; *Wear*. (1995) 443-457

Aurelie Roauaix- Vande, Kinga A. Unocic and Michael P. Brandy. "Performance of chromia- and alumina-forming Fe- and Ni-base alloys exposed to metal dusting environments: The effect of water vapor and temperature" *Corrosion Science, El Sevier.* 92. (2015).

S.N. Karlsdottir, K.R. Ragnarsdottir, I.O. Thorbjornsson and A. Einarsson. (June 2014). "Corrosion testing in superheated geothermal steam in Iceland". *El Sevier,* 53, 281-290.

I. Thorbjornsson. "Corrosion fatigue testing of eight different steels in an Icelandic geothermal environment". *Materials & Design.* 16-2. (1995).

Heber Diez. Abrasión por Partículas en Suspensión en Pozos Geotérmicos productores de Ultra Alta Entalpía. TESIS de Maestría. Mayo de 2018.

Heber Diez. Informe Interno Comisión Federal de Electricidad (CFE), junio de 2019.